

An Integrated OFDM Receiver for High-Speed Mobile Data Communications

Hanli Zou, Bruce McNair* and Babak Daneshrad

Wireless Integrated Systems Lab
Department of Electrical Engineering
University of California, Los Angeles
e-mail: babak@ee.ucla.edu

* Wireless Systems Research Dept.
AT&T Labs-Research
Middletown, New Jersey 07748
e-mail: bmcnair@research.att.com

Abstract—In this paper, we present the system design of an integrated receiver for the next generation high-speed mobile data communications based on OFDM. First an overview of the OFDM system suitable for mobile communications is described. The effects of non-ideal transmission conditions of the OFDM system including channel estimation errors, symbol timing offset, carrier and sampling clock offset, phase noise and time-selective fading are analyzed. We then propose an integrated receiver in which all of these issues relevant to the mobile transmission environment are addressed. Novel techniques for symbol timing and frequency synchronization are proposed. The architecture of the receiver and resulting implementation complexity are then analyzed. The overall performance of the proposed receiver is simulated and evaluated in various channel conditions.

I. INTRODUCTION

Orthogonal Frequency Division Multiplexing (OFDM) is well known as a highly spectral efficient transmission scheme capable of dealing with severe channel impairments encountered in mobile environment [1]. OFDM has been chosen as the air interface standards for digital audio broadcasting (DAB) [2] and digital terrestrial television broadcasting (DVB-T) [3] in Europe which support digital broadcasting at megabits data rates. It is also the physical layer modulation scheme chosen by the IEEE 802.11a standard to allow wireless LANs operating at bit rates up to 54 Mb/s at 5 GHz. OFDM also found applications in broadband fixed wireless access.

OFDM can largely eliminate the effects of inter-symbol interference for high-speed transmission in highly dispersive channels with a relatively low implementation cost by separating a single high speed bit stream into a multiplicity of much lower speed bit streams each modulating a different sub-carrier. Recently there is a growing interest in applying OFDM to provide high-speed data access in mobile cellular systems [4]. However OFDM is known to be vulnerable to synchronization errors due to the narrow spacing between sub-carriers. Additionally in order to achieve high spectrum efficiency coherent demodulation with multi-level modulations such as QAM is employed which mandates accurate channel estimation and tracking in the receiver. There exist many publications dealing with the synchronization and channel estimation issues of OFDM receiver. However, a majority of the work addressed the fore mentioned problems for different applications, with even fewer works lend them readily to integrated circuit implementations suitable for mobile handheld devices. In this paper, we take an integrated approach to thoroughly analyze the impairments due to synchronization, imperfect channel

estimation as well as receiver analog components imperfections encountered in applying OFDM to mobile cellular environments. In particular, we consider the algorithms with the assumption that they can be readily implemented in low cost and low power integrated circuits or digital signal processors (DSP).

In this paper, we first introduce an OFDM system structure suitable for mobile applications in section II. Then the impairments due to non-ideal transmissions are analyzed in section III. The proposed receiver architecture is presented and the achievable performance and resulting receiver complexity are quantified in section IV. Computer simulation results of the complete receiver in a variety of channel conditions will be presented afterwards, followed by the conclusion.

II. OFDM SYSTEM MODEL

The objective of the OFDM receiver is to synchronize and demodulate the signal properly and then hand the soft and hard decisions to the outer receiver for further processing such as diversity combining, deinterleaving and channel decoding.

A. OFDM Signal Model

An OFDM system forms its symbol by taking K complex QAM symbols $X_{l,k}$ each modulating a sub-carrier with frequency $f_k = k/T_u$ where T_u is the sub-carrier symbol period. The modulation is accomplished by means of an N -point (N^2K) IFFT with a sampling period of $T = T_u/N$. A pulse-shaping filter $g(t)$ is used to further limit the transmission spectrum. To avoid intersymbol interference (ISI) caused by the channel multipaths, a cyclic prefix of length $T_g = N_g T$ is pre-appended to the OFDM symbol thus the transmitted complex baseband signal is described by

$$x(t) = \frac{1}{\sqrt{T_u}} \sum_{l=-\infty}^{+\infty} \sum_{k=-K/2}^{K/2-1} X_{l,k} e^{j2\pi f_k(t-T_s-lT_o)} g(t-lT_o) \quad (1)$$

where $T_o = T_g + T_u$ is the resultant OFDM symbol period corresponding to $N_o = N_g + N$ samples.

The signal is transmitted over a frequency selective multipath fading channel and sampled at the receiver to yield

$$y(nT) = \sum_{m=0}^{M-1} h_m(nT)x(nT - \mathbf{t}_m) + n(nT) \quad (2)$$

where $h_m(t)$ is the equivalent low pass impulse response for the m -th multipath component. It is assumed that the channel impulse response is quasi static during one symbol period. The cyclic prefix is chosen to be longer than the maximum channel multipath delay so that the current symbol is not contaminated by previous symbols. Assuming perfect

receiver synchronization, stripping away the cyclic prefix and applying an N -point FFT yields the demodulated sub-carrier symbols

$$Y_{l,k} = X_{l,k}H_{l,k} + \tilde{n}_{l,k} \quad (3)$$

where $H_{l,k} = \sum h_{l,m} e^{-j2\pi f_k t_m}$ is the channel frequency response at sub-carrier frequency f_k during the l -th symbol. Assuming $E\{|X_{l,k}|^2\} = E\{|H_{l,k}|^2\} = 1$ and the sampled AWGN $\tilde{n}_{l,k}$ has variance of σ_n^2 , the signal to noise ratio (SNR) per sub-carrier symbol is then $SNR = 1/\sigma_n^2$

B. Wideband OFDM Testbed

To demonstrate the feasibility of a flexible, low-cost and robust OFDM-based system that could be employed in future mobile systems, a wideband OFDM testbed is currently being developed. Figure 1 illustrates the detailed frame structure used in the testbed. Five OFDM symbols transmitted in 1 ms comprise one signaling unit or burst. A long burst guard interval follows the last symbol which eliminates any ISI between adjacent bursts.

Dedicated pilot symbols are embedded in the 2nd and 4th OFDM symbols as shown in Figure 2 where D_t and D_f indicate the distance between pilots in the time and frequency direction respectively. The pilot symbols are BPSK modulated and derived from a maximum length binary sequence (MLBS) with the polynomial $G(D) = D^{10} + D^3 + 1$. TABLE 1 summarizes the basic transmission parameters of the OFDM testbed system in our study. The 1024 IFFT samples represent the transform of maximum 640 QPSK modulated sub-carriers. The sub-carrier spacing is 6.35kHz and the total bandwidth is thus 4 MHz. The OFDM symbol length is 188.3 μ s after appending a cyclic extension of 30.8 μ s. The maximum raw channel data rate is 2.56 MBaud. With QPSK modulation and rate $\frac{1}{2}$ channel coding plus framing and control overhead, this can easily attain a peak end user capacity of 2 Mb/s.

III. EFFECTS OF NON-IDEAL TRANSMISSION

A variety of impairments exist in an OFDM transmission system that could cause performance degradation. Among them, symbol timing offset, carrier frequency and sampling clock frequency offset, phase noise and time-variant channels are the ones that need special attention, as the receiver performance heavily depends on them.

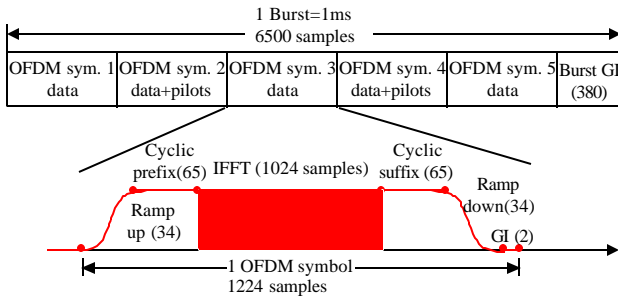


Figure 1 Testbed frame structure

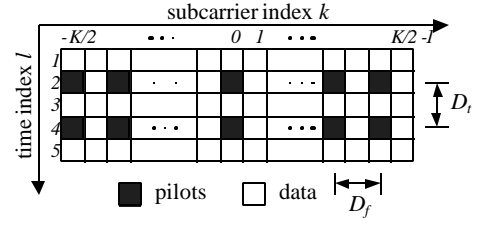


Figure 2 Pilot symbol pattern

TABLE 1

OFDM SYSTEM PARAMETERS

N	N _g	1/T	T _u	1/T	K	Modulation
1024	200	6.5 MHz	157.5 μ s	6.35 kHz	640	QPSK

A. Symbol Timing Offset

The timing synchronization unit of the receiver performs the task of identifying the correct symbol start and removal of the cyclic prefix/suffix. As illustrated in Figure 3, as long as the FFT window start position falls within the allowed region no ISI occurs. Under this condition, the presence of a positive symbol timing offset $\Delta t = \Delta nT$ causes the FFT output to become

$$Y_{l,k} = X_{l,k}H_{l,k}e^{-j2\pi \frac{k\Delta n}{N}} + \tilde{n}_{l,k} \quad (4)$$

It is evident that the presence of timing offset causes a phase rotation proportional to the sub-carrier index k and the timing offset Δn . However, if the timing offset causes the FFT window start position to fall outside the allowed region, both ISI and inter-carrier interference (ICI) occurs due to the disturbance of adjacent symbols. The post-FFT signal is then given by [5]

$$Y_{l,k} = e^{-j2\pi \frac{k\Delta n}{N}} \mathbf{a}(\Delta t) X_{l,k}H_{l,k} + \tilde{n}_{l,k} + n_{\Delta t;l,k} \quad (5)$$

where the ISI and ICI are modeled as additional noise $n_{\Delta t;l,k}$ while the attenuation is $\mathbf{a}(\Delta t)$ close to 1 for large N .

B. Carrier and Sampling Clock Frequency Offset

The effect of carrier frequency offset in OFDM is analyzed in detail in [5][6]. Assume in addition to a frequency offset of $\Delta k = \Delta fT_u$, $y(t)$ is sampled at an interval of $\tilde{T} = (1+\mathbf{d})T$ where \mathbf{d} is the sampling clock frequency offset. The FFT output becomes

$$Y_{l,k} = X_{l,k}H_{l,k} \frac{\sin \mathbf{p}\mathbf{e}}{N \sin(\mathbf{p}\mathbf{e}/N)} e^{j\mathbf{p}\mathbf{e}(N-1)/N} + n_{\Delta f;l,k} + \tilde{n}_{l,k} \quad (6)$$

where $\mathbf{e} = \Delta k(1+\mathbf{d}) + k\mathbf{d}$ and the ICI noise term is given by

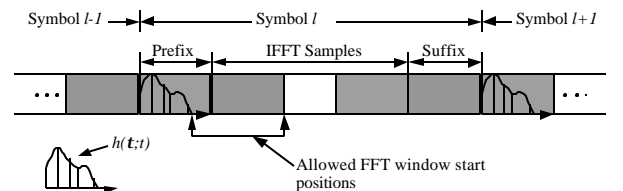


Figure 3 Symbol timing synchronization scenario

$$n_{\Delta f;l,k} = \sum_{m=-K/2, m \neq k}^{K/2-1} X_{l,m} H_{l,m} \frac{\sin \mathbf{p}(m-k+\mathbf{e})}{N \sin(\mathbf{p}(m-k+\mathbf{e})/N)} e^{j\mathbf{p}(m-k+\mathbf{e})(N-1)/N} \quad (7)$$

The effects of carrier and sampling clock frequency offset are two folded. One is the extra phase shift that can be translated into a normalized frequency offset of $\Delta k + k\mathbf{d}$ (assuming \mathbf{d} is small and N is large). Thus sampling clock frequency offset leads to an additional frequency offset that is proportional to \mathbf{d} and sub-carrier index k . For our system, assuming a sampling clock frequency offset of 100ppm ($\mathbf{d} = 10^{-4}$) and $K = 640$, the maximum additional frequency offset is ± 0.032 times sub-carrier spacing at the edge of the band and the resultant phase rotation could be compensated by the channel estimator. The other effect due to frequency offset is the reduction of useful signal energy though it is small in tracking mode. Through simulation and analysis we found a residue frequency error of less than 1-2% of sub-carrier spacing is required.

C. Effects of Phase Noise

OFDM has been shown to be sensitive to the phase noise in the oscillators. The effects of oscillator phase noise are two folded as shown in [7]. The first consequence due to phase noise is the loss of orthogonality between sub-carriers. The resultant ICI noise power on each sub-carrier is upper-bounded by [7]

$$\mathbf{s}_{pn}^2 \leq \sum_{k=-K/2, k \neq 0}^{K/2-1} \int_{-\infty}^{\infty} L_{\Phi_n}(f - [f_k - f_0]) \text{Sinc}^2(\mathbf{p}f T_u) df \quad (8)$$

where $\text{Sinc}(x) = \sin x/x$. Thus the ICI noise power depends on the shape of the phase noise spectrum $L_{\Phi_n}(f)$ and increases with the number of sub-carriers K .

The second effect due to phase noise is the so-called common phase error (CPE) [7]. In addition to the ICI, a common phase drift Φ_E that is only a function of the OFDM symbol index l also modulates each sub-carrier. Usually a near-in phase noise level less than -60 dBc/Hz is required such that perturbation due to CPE is minimal.

D. Effects of Time Varying Channel

One major perturbation to the channel estimation is the loss of orthogonality among sub-carriers due to time-variant channels. The assumption that $h(\mathbf{t}; t)$ is constant during one OFDM symbol is no longer true in fast fading environments. Several publications have analyzed this effect [5][8]. The received sub-carrier symbols in this case should be revised as

$$Y_{l,k} = X_{l,k} H_{l,k} + \tilde{n}_{l,k} + n_{fad;l,k} \quad (9)$$

where the additional ICI noise $n_{fad;l,k}$ is caused by the time-variant channel and $H_{l,k}$ is the average channel gain factor.

The power of the ICI noise caused by a band-limited fading channel with the Jakes Doppler spectrum is lower bounded in [5] by

$$\mathbf{s}_{fad,l}^2 \approx \frac{\mathbf{p}^2}{6} (f_D T_u)^2 \quad (10)$$

where f_D is the maximum Doppler frequency. From the equation it is calculated that a maximum normalized Doppler frequency of 0.02 (which corresponds to $f_D = 130$ Hz) can be tolerated without significant performance loss at high SNR values.

IV. RECEIVER ALGORITHMS

In this section, we outline the OFDM mobile receiver synchronization and channel estimation strategies based on the above analysis.

A. Synchronization

The synchronization unit for OFDM receivers can extract the synchronization information either before or after demodulating via the FFT. Pre-FFT synchronization methods have the advantage of faster synchronization and less power consumption without the computation burden of the FFT. Post-FFT methods are more accurate, though they require a long iteration process to accomplish acquisition and the performance is adversely affected if the orthogonality between sub-carriers is not established. From the system design point of view it is beneficial that both pre-FFT and post-FFT synchronization methods be employed in a burst transmission system in order to achieve both rapid acquisition and accurate tracking.

1. Pre-FFT Synchronization

Since no specific training data or preamble is sent prior to the OFDM symbols in the testbed system, only non-data-aided (NDA) pre-FFT synchronization methods are considered here. A modified block diagram of the original guard interval based synchronization algorithm [9] is illustrated in Figure 4.

The maximum likelihood estimate of the normalized frequency offset at time instant n is given by

$$\Delta \hat{k} = \frac{1}{2\mathbf{p}} \arg \left(\sum_{k=n-N_g+1}^n y_k y_{k-N}^* \right) \quad (11)$$

and the symbol start position \hat{n} can be estimated using the amplitude of the correlation value as shown below

$$\hat{n} = \arg \max_n \left| \sum_{k=n-N_g+1}^n y_k y_{k-N}^* \right|^2 \quad (12)$$

The pre-FFT synchronization algorithm can be significantly simplified if only the sign bit of the samples is used in the correlation [9]. Further simplification could be achieved by using sum of the absolute value of the real and imaginary parts of samples instead of using the amplitudes. However the accuracy of this pre-FFT symbol timing estimation is not enough for fine tracking though they can still be effectively used in coarse timing acquisition. Fine timing tracking is handled after taking the FFT.

Although the frequency-offset estimate is quite accurate using this scheme, the detection range is limited to half of the sub-carrier spacing due to phase ambiguity. The issue of detecting the integer frequency offset is best resolved in the frequency domain after taking the FFT.

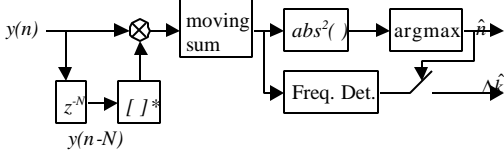


Figure 4 Block diagram of pre-FFT synchronization

2. Post-FFT Synchronization

First proposed by McNair in [10], the post-FFT fine timing synchronization is carried out in the frequency domain based on measuring the phase difference between adjacent sub-carrier symbols. Figure 6 illustrates the block diagram of the post-FFT timing synchronization unit.

Using the pilots to remove the modulation, the timing offset Δn can be accurately estimated as follows

$$\Delta \hat{n} = -\frac{N}{2pD_f} \arg \left(\sum_{i=2}^p Z_{l,p_i} Z_{l,p_{i-1}}^* \right) \quad (13)$$

Through simulation, we found using fewer (1/2 or 1/4) pilots also gives good results. Non-data-aided method of removing the modulation is also possible by passing the data through a non-linear operator. The performance of the post-FFT timing estimator is plotted in Figure 5.

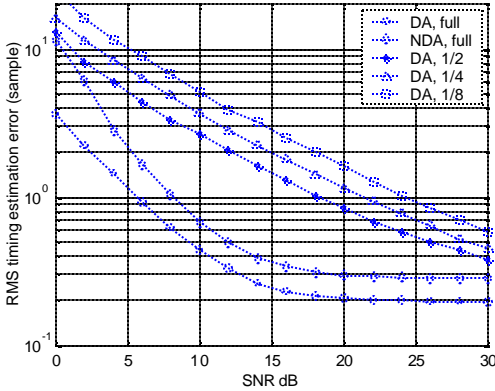


Figure 5 RMS error of the post-FFT timing estimator in TU channel

A block diagram for estimating the integer frequency offset is shown in Figure 7. By correlating the received pilot symbols with a shifted version of the original pilots, the integer frequency offset can be identified with high probability. The effect of frequency selective channel is removed by the complex conjugate multiplication between two adjacent sub-carriers. TABLE 2 demonstrates the missed lock probability of the post-FFT integer frequency offset estimator using half of the pilots is less than 1% in various channels with an SNR of less than 4 dB.

TABLE 2

MISSED-LOCK PROB. OF POST-FFT FREQUENCY ESTIMATOR

SNR (dB)	0	2	4	6	8
TU	0.0095	0.0015	0	0	0
HT	0.027	0.008	0.0025	0.001	0
2-ray (10 μ s)	0.054	0.0215	0.007	0.004	0.0015

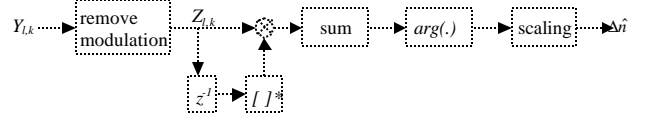


Figure 6 Block diagram of post-FFT timing estimation

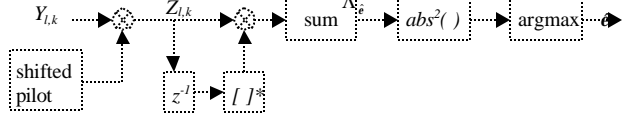


Figure 7 Integer frequency offset estimator

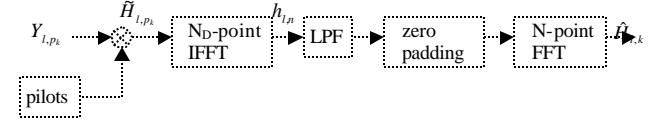


Figure 8 1-D FFT/IFFT based channel estimation

B. Channel Estimation

We assume all the channel multipaths are Rayleigh distributed according to the Jakes spectrum with maximum Doppler frequency f_D . The sampling theorem requires that the sampling rate in the time and frequency direction must satisfy

$$1/T_s(D_f T_o) > 2(f_D + \Delta f) \quad (14)$$

$$T_u/D_f > 2t_{\max} \quad (15)$$

where t_{\max} is the maximum channel delay spread and f_D is the frequency offset.

A 1-D FFT/IFFT based estimator is proposed in [11] while in [12] Li proposes a robust channel estimator using 2-D FFT and IFFT. Our channel estimation is a compromise of the two methods in which a 1-D FFT/IFFT based channel estimator is applied to the pilot sub-carriers followed by linear time domain interpolation.

Figure 8 illustrates the block diagram of the 1-D FFT/IFFT based channel estimator. After an initial estimation of channel transfer functions on the pilot sub-carriers, a robust interpolation is applied to estimate the channel parameters for all other sub-carriers. Instead of using the Wiener filter approach, we adopt a transform domain filtering and interpolation method, which is less dependent on channel statistics. The low pass filter applied after the IFFT is a brick wall type filter which does ideal interpolation.

After the 1-D FFT based interpolation in frequency direction, simple linear interpolation is carried out in the time direction. Channel transfer functions for symbol 1, 3 and 5 are linearly interpolated/extrapolated using the estimates obtained from symbol 2 and 4. Since the pilots are separated by 2 in time direction, only simple shifter and adder are needed to accomplish this interpolation.

V. RECEIVER ARCHITECTURE AND PERFORMANCE

In this section, we present the final receiver architecture as well as its performance in various mobile channels.

A. Receiver Architecture

The final architecture of the OFDM receiver based on the algorithms proposed in Section IV is shown in Figure 9. The IF signal is sampled at 26 MHz, then digitally downconverted and decimated to baseband through the I/Q demodulator. Both the pre-FFT and post-FFT synchronization units are adopted to provide fast coarse acquisition as well as fine tracking. Channel estimation based on the 1-D FFT/IFFT plus linear time interpolation is efficiently implemented by reusing the FFT/IFFT engine.

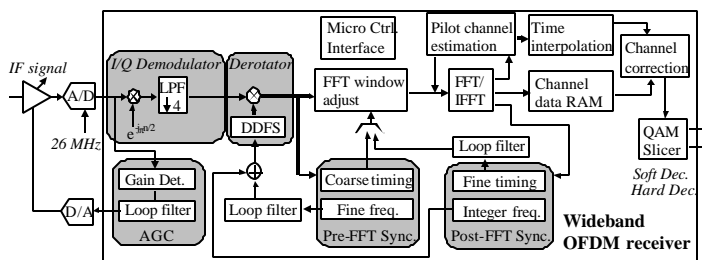


Figure 9 Wideband OFDM receiver architecture

B. Receiver Performance

The complete OFDM receiver architecture has been simulated with the synchronization (timing, frequency and AGC) loops in dynamic and the proposed 1-D FFT/IFFT based channel estimation and correction algorithm. Various mobile channel (TU and HT) profiles have been applied to test the robustness of the receiver. Throughout the simulation we have assumed a frequency offset of $\Delta f T_u = 0.1$ and the transmit timing is unknown at the receiver. The performance achieved with perfect channel estimation and synchronization is also plotted as a comparison.

As shown in the next figures, the performance loss of the proposed receiver is 2 to 2.5 dB with respect to the ideal receiver. Also we note that the receiver is very robust to Doppler frequency. The degradation from low (40 Hz) to high (200 Hz) Doppler frequency is negligible.

VI. CONCLUSION

In this paper, a complete OFDM receiver architecture suitable for high-speed mobile wireless communications has been proposed. The key computation blocks of the receiver suitable for VLSI implementations are also identified. The proposed architecture exhibits robust performance in various mobile channels with high Doppler frequency. Such a receiver will be incorporated on a testbed and used in field trial to demonstrate the feasibility of high-speed mobile data access based on OFDM for the next generation cellular system.

REFERENCES

- [1] S. B. Weinstein and P. M. Ebert, "Data transmission by frequency-division multiplexing using the discrete Fourier transform," *IEEE Trans. Commun. Technol.*, Vol. COM-19, Oct. 1971, pp. 628-634.
- [2] M. Alard and R. Lassalle, "Principles of modulation and channel coding for digital broadcasting for mobile receivers," *EBU Tech. Review*, no. 224, Aug. 1987, pp. 168-190.

- [3] U. Reimers, "Digital video broadcasting," *IEEE Commun. Mag.*, Vol. 36, No. 6, June 1998, pp. 104-110.
- [4] J. Chuang and N. Sollenberger, "Beyond 3G: wideband wireless data access based on OFDM and dynamic packet assignment," *IEEE Commu Mag.*, Vol. 38, No. 7, July 2000, pp.78-87.
- [5] M. Speth, S. Fechtel, G. Fock, and H. Meyr, "Optimal receiver design for wireless broad-band systems using OFDM-part I," *IEEE Trans. Commun.*, Vol. 47, No. 11, Nov. 1999, pp. 1668-1677.
- [6] T. Pollet, M. Ven Bladel, and M. Moeneclaey, "BER sensitivity of OFDM systems to carrier frequency offset and Wiener phase noise," *IEEE Trans. Commun.*, Vol. 43, Feb./Mar./Apr. 1995, pp. 191-193
- [7] P. Robertson and S. Kaiser, "Analysis of the effects of phase noise in orthogonal frequency division multiplex (OFDM) systems," *Proc. ICC'95*, June 1995, pp. 1652-1657.
- [8] P. Robertson and S. Kaiser, "Analysis of the loss of orthogonality through Doppler spread in OFDM systems," *Proc. GLOBALCOM'99*, Nov 1999, Part B, pp. 701-706.
- [9] J.-J. van de Beek, M. Sandell, M. Isaksson, and P. Borjesson, "Low-complex frame synchronization in OFDM systems," in *Proc. ICUPC*, Nov. 1995, pp. 982-986.
- [10] B. McNair, L. J. Cimini, Jr., and N. R. Sollenberger, "A robust timing and frequency offset estimation scheme for orthogonal frequency division multiplexing (OFDM) systems," in *Proc. VTC'99*, June 1999, pp. 690-694.
- [11] Y. Zhao and A. Huang, "A novel channel estimation method for OFDM mobile communication systems based on pilot signals and transform-domain processing," *Proc. VTC'97*, vol. 3.3, pp. 2089-2093.
- [12] Y. Li, "Pilot-symbol-aided channel estimation for OFDM in wireless systems," *Proc. IEEE VTC'99*, pp. 1131-1135.

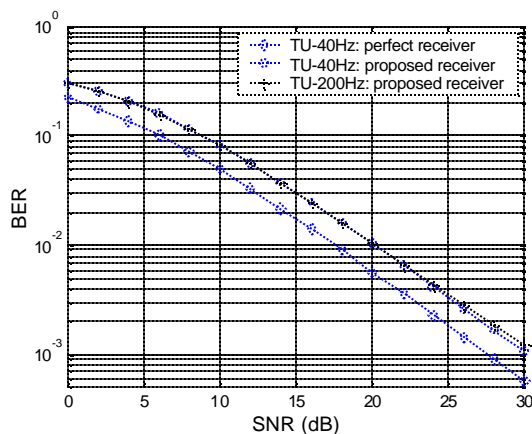


Figure 10 BER of ideal and proposed receiver in TU channel

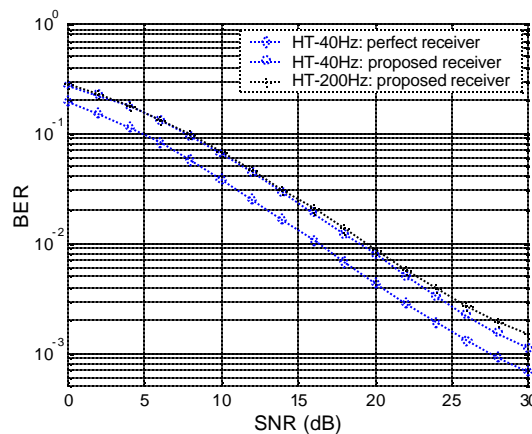


Figure 11 BER of ideal and proposed receiver in TU channel